Plastic Deformation of Metal/Ceramic Nanolayered Composites

I. SALEHINIA,[1,3] S. SHAO,[2] J. WANG,[2] and H.M. ZBIB[1]

1.—School of Mechanical and Materials Engineering, Washington State University, Pullman, WA 99164-2920, USA. 2.—Materials Science and Technology Division, Los Alamos National Laboratory, Los Alamos, NM 87545, USA. 3.—e-mail: iman.salehinia@email.wsu.edu

Metal/ceramic multilayers combine high hardness of the ceramic layer and the high ductility of the metallic layer, enabling the design of novel composite coatings with high hardness and measurable ductility when the layer thickness reduces to a few nanometers. In this article, we review recent work with a focus on plastic deformation of metal/ceramic nanolayered composites from three aspects: experiment, theory, and atomistic modeling, and we propose several research directions in this topic.

INTRODUCTION

Recent advances in energy and defense-related technologies and aerospace engineering entail developing a new class of materials that can efficiently perform without premature failure under extreme loading and harsh environmental conditions. These materials are engineered to compensate for the deteriorating effect of structural and chemical defects that are inevitable in materials. In recent years, metal/ceramic multilayers have come into greater focus due to their promising mechanical, physical, and chemical properties, making them practically useful for harsh environments and extreme loading.[1] These composites show improvement in hardness, toughness, wear resistance, thermal resistance, shock resistance, and irradiation resistance, to name a few. In this article, we summarize recent studies of metal/ceramic multilayers with focus on plastic deformation from three aspects: experiment, theory, and modeling. Scrutinizing the available data in the literature, we also suggest several future research topics on the mechanical properties of metal/ceramic multilayers.

EXPERIMENTAL STUDIES OF METAL/ CERAMIC MULTILAYERS

A broad range of metal/ceramic layered composites have been extensively tested in experiments, including transition metal nitrides/metal (TiN/W,[2] TiN/Al,[3–5] TiN/Ti,[6–10] NbN/Mo,[11–13] NbN/W,[11,13,14] ZrN/W,[13,15,16] WN/W,[7] HfN/Hf,[7] TiN/Cu[17]), transition metal carbides/metal (TiC/Fe,[18,19] TiC/W,[19] WC/Ni,[20] WC/Co,[20] TiC/Cu,[19] TiC/Al,[19] TiC/Mo[21]), oxide/metal (Al_2O_3/Ni,[22] Al_2O_3/Al[23]), metal-nitrides/metal (AlN/W,[24] AlN/Al[25,26]), SiC/metal,[27–35] and diamond-like carbon (DLC)/metal[36] multilayer composites. The mechanical properties of metal/ceramic layered composites have been studied under various types of loading including compression,[5,31] tension,[27] and nanoindentation[2–4,6,9,21,26,28,32,33] normal to the interface. It has been recognized that enhancement in both hardness and ductility is achieved compared with the rule of mixture values (Fig. 1).

The bilayer thickness and the thickness ratio between the ceramic and metal layers greatly affect the hardness and ductility of layered composites. Studies show that for thick layers (>10 nm), while the metallic layer can undergo elastic–plastic deformation, the ceramic layer remains in the elastic regime until it is failed due to cracks,[3] or highly localized shear deformation may form as a result of localized stresses at the interface.[1,13,16,37] Figure 2 shows plastic deformation in Al layers and crack in TiN layers in TiN/Al multilayers[3] (Fig. 2a, b), and plastic deformation in W layers and twin-like features as straight lines in NbN layers in NbN/W multilayers[13] (Fig. 2c). In a nanoscale regime, experimental measurements demonstrate that ceramics could plastically codeform with metals when layer thickness reduces to a few nanometers.[3,38] Hardness often reaches a peak by varying the bilayer period (wave length) of multilayer metal/ceramic composites. Shih and Dove[7] studied the various metal/ceramic combinations with bilayer period ranging from 4 nm to 200 nm. They found that the maximum hardness for TiN/Ti, HfN/Hf, and WN/W multilayered composites correspond to the bilayer period of 16 nm, 8 nm, and 36 nm, respectively. They also reported no decrease

in hardness of HfN/Hf and WN/W by decreasing the bilayer period from that corresponding to the peak hardness. Given the bilayer period of multilayers, the metal/ceramic thickness ratio also influences mechanical properties of multilayers. It has been seen that the hardness decreases with increasing metal/ceramic thickness ratio.[4,19]

It has been observed that the strength seems to have strong dependence on the combination of materials, while the improvement in ductility is commonly observed in most ceramic/metal multilayers.[2–5,13,16,17,19] He et al.[19] showed an improvement in toughness for most TiC/metal layered composites compared with single-crystal TiC, but no improvement in hardness was reported for TiC/Al and TiC/Cu layered composites. This anomaly has also been reported for TiN/Cu[17] and ZrN/W[16] multilayers. However, Bhattacharyya et al. reported
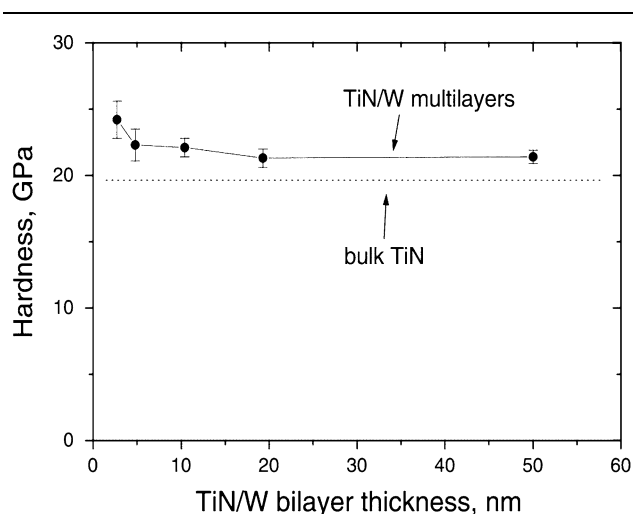

Fig. 1. Hardness versus bilayer thickness for TiN/W multilayers. Hardness is larger than the rule-of-mixture value and it is lower for larger bilayer period.[2]

enhancement of both hardness and ductility for TiN/Al using nanoindentation and micropillar compression tests when both layers thickness is in a region of a few nanometers.[3–5] Although several explanations have been used in the field, none of them are universally applicable. Barnett and Madan[13] and Abadias et al.[17] associated the lack of hardness enhancement in TiC/Cu, TiC/Al, and TiN/Cu multilayers to the low yield strength and high dislocation activities in metallic layer as the level of stress equal to the theoretical strength results in its early failure. Abadias et al.[16] linked the lack of improvement in hardness of ZrN/W to two main sources, i.e., easier dislocation glide from the metallic layer to the ceramic layer due to a small difference between the shear moduli of ZrN and W (Koehler's theory) and the delamination due to compressive stresses in the composite structure under nanoindentation loading. However, in a separate study, Abadias et al.[2] reported hardness greater than the rule of mixture for TiN/W multilayers despite a small difference between the shear moduli of TiN and W, and they linked it to the sharp and smooth interface barrier between the metallic and ceramic layers.

Therefore, the experimental discovery regarding the improvement in strength and ductility of the metal/ceramic multilayers depending on the several factors demands a better theoretical understanding of the deformation mechanisms of such materials. This is especially the case when obvious disagreement exists among the researchers regarding the dependence of strength on the material system including crystal structures, difference in shear moduli, and difference in theoretical yield strength values of the metallic and ceramic layers. Future studies will explore the effect of various crystal structures, difference in shear moduli and dislocation line energy, and difference in theoretical yield strength of the metallic and ceramic layers on the overall mechanical behavior of multilayer metal/ceramic composites.
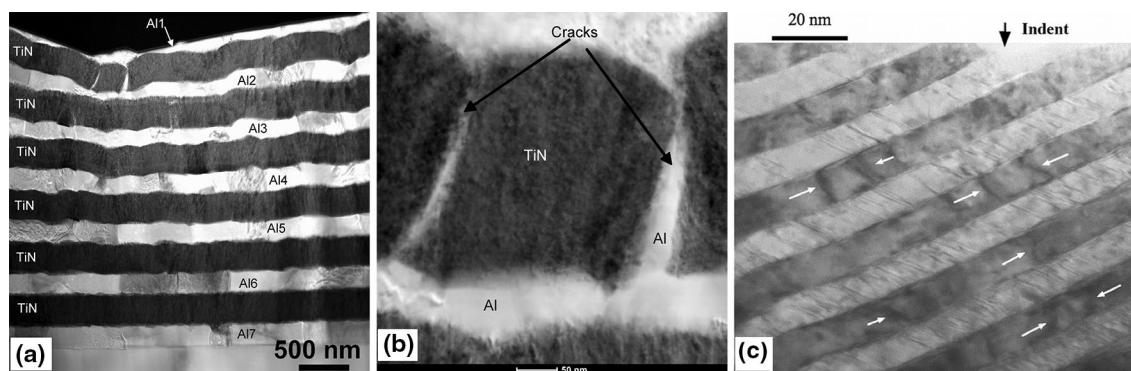

Fig. 2. (a, b) Scanning electron microscopy (SEM) images of deformation mechanisms in Al and TiN when the multilayer is being indented by a Berkovich tip. Al layers carry out plastic deformation by dislocation glide, while TiN layers behave less ductile and show cracks. Cracks are filled by Al layer.[3] (c) Transmission electron microscopy (TEM) micrograph of nanoindentation on 10 nm W/10 nm NbN multilayers showing plastic deformation in W layers and twin-like features as straight lines in NbN layers.[13]

THEORETICAL MODELS

In metal/ceramic multilayer composites, dislocations are initially generated in the more compliant (metal) layer and then transmitted to the harder layer. According to the confined layer slip deformation mechanisms in layered composites, strain hardening in nanolayered composites generally occurs when dislocations glide and interact in a single layer, and higher stresses are required to transmit them into the other layer. The transmission of dislocations also gives rise to ductility in the multilayer. Therefore, the strength and ductility of the multilayers ultimately depends on the difficulty to thread a dislocation within a layer and/or to transmit a dislocation across the interface. The factors governing the strength and ductility discovered in the experiments (material choice, bilayer thickness, and layer thickness ratio) are only realized by affecting the propagation and transmission behavior of dislocations during deformation.

Hardening of the multilayer that is mainly due to the propagation and impediment of threading dislocation within the metal layers is affected by several factors, such as the thickness of the metal layer and the thickness ratio between metal and ceramic layers. Based on confined layer slip mechanisms, Nix[39] calculated the yield strength of a bilayer (soft metal film on a rigid substrate) as a function of metal film thickness by assuming that a gliding dislocation is forced by the elastic field of the substrate to pass through the metal film at some standoff distance away from the interface. Anderson and Kreidler [40,41] and Embury and Hirth[42] also studied strain-hardening mechanisms of metal-ceramic/amorphous multilayers based on the interaction of a glide dislocation loop and deposited dislocations at interface. Wang and Misra[38] analyzed the dependence of strain hardening on the layer thickness and the layer thickness ratio in ceramic/metal multilayer composites using a three-dimensional crystal elastic–plastic model that describes plastic deformation according to the confined layer slip mechanism. The high strain-hardening rate was linked to the closely spaced deposited dislocations at interfaces and the load transfer that is related to the layer thickness ratio of metal and ceramic layers. Under compressive loading normal to the interface, the resulting resolved shear stress drives the threading dislocations to propagate within the metallic layer. Because of the large difference in the dislocation activities between the metallic and ceramic layers, more dislocations in metal layers pile up and/or accumulate at the interface. Because of the displacement compatibility at the interface, this loading condition generates compressive stresses in the metallic layer and tensile stresses in the ceramic layer parallel to the interface (Fig. 3a). Moreover, the compressive stress in the metallic layer reduces the resolved shear stress required for dislocation propagation and consequently results in the strain hardening. The compressive stress is dependent on the thickness ratio between the metal and ceramic layers.

The dislocation transmission is dependent on both the material choice and the metal layer thickness. The material choice determines several factors such as crystal structure, dislocation-line energies, and stacking-fault energies of the constituent crystals, all of which affect the transmission of dislocations. The interface structure is governed by the crystal structures of the metal and ceramic layers. When the interface structure is coherent, high-coherency stresses make dislocation transmission difficult.[43] On the other hand, the weak shear resistance of incoherent or semicoherent interfaces facilitates the core spreading of dislocations on the interface. For these interfaces, lattice dislocation can be smeared over the interface because of the thermodynamical reconstruction of the interface.[44] The dislocation-line energies and stacking-fault energies in the crystals determine the energy barrier of the transmission process, which governs difficulty of the transmission.

During plastic deformation, lattice dislocations in metal layers may deposit at the interface. According to Wang and Misra,[38] under compressive loading normal to the interface, the tensile stress generated in ceramic layers favors slip and cracking. The deposited dislocations on interfaces increase the local stresses in the interface and consequently facilitate nucleation of lattice dislocation in the adjacent layer (Fig. 3b). Wang and Misra[38] showed that local stresses due to deposited dislocation are higher for thinner ceramic layers. Therefore, the small thickness of the ceramic layer is crucial for the codeformation of both layers.

Barnett and Madan[13] performed an extensive study on the mechanical properties of metal/nitride multilayer composites at low and high temperatures. They attempted to link the experimental trends to the available models and deformation mechanisms. For instance, because of the close value of power m in the Hall–Petch formula in their work ($m = 0.38 \pm 0.03$) and that in the model developed by Andersonand Li[37] (0.3), they linked the yielding in ceramic layer to the dislocation nucleation at the head of the dislocation pileup at the interface. In the other words, they replaced the interface barrier stress in the Anderson and Li's model by the critical stress for dislocation nucleation. Barnett and Madan[13] discussed another possible explanation for the trend of hardness versus bilayer period based on two separate mechanisms: glide of dislocation loops within the individual layers (working for bilayer period of greater than 20 nm) and approaching the theoretical strength of the metallic layer (for bilayer period of less than 20 nm). A model where dislocation loops can propagate within the individual layers provides a good agreement with the experimental data for bilayer period of larger than 20 nm, but it overestimates the hardness for bilayer period of less than 20 nm. The predicted hardness by this model devi-
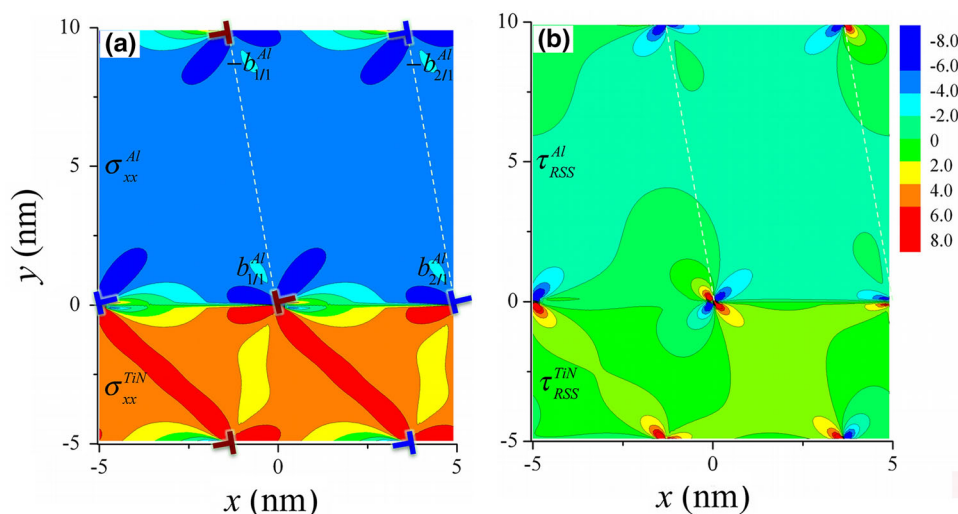
Fig. 3. Stress fields in 10 nm Al/5 nm TiN due to deposited interface dislocations: (a) the normal stress parallel to the interface and (b) the resolved shear stress with respect to a glide plane (denoted as dashed white lines).[38] (Stress values are in GPa.)

ates from the experimental data at around the hardness of the metallic layer. The hypothesis was that by decreasing the bilayer period from 20 nm, the strength of the metallic layer remains constant and the theoretical resolved shear stress of the ceramic layer is much bigger than that of the metallic layer. This results in increase of the hardness of the multilayer but at a slower rate than predicted by the model.

The theoretical models assumed a higher nucleation stress for lattice dislocations than the threading stress of existing dislocations. However, when the metallic layer is thin enough or in dislocation-starved conditions, the nucleation of lattice dislocations dominates the plastic deformation. Being dependent on the misfit dislocation structure, the mechanisms of dislocation nucleation need to be carefully addressed by atomistic simulations.

ATOMISTIC MODELING

In parallel to theoretical and experimental studies, atomistic simulations provide insights into understanding plastic deformation in metal/ceramics multilayers. Atomistic modeling approaches, including ab initio[45–59] and molecular dynamics methods,[60,61] have been used mainly to study the interface properties of metal/ceramic pairs. We have recently applied molecular dynamics to explore the atomic mechanisms of plastic deformation in Nb/NbC nanolayered composites. What follows is a brief summary of the interface structure, plastic deformation mechanisms, and influence of layer thickness ratio on mechanical behavior of Nb/NbC nanocomposite.

Interface Structure

Interfaces can act as sources, sinks, and barriers for point and line defects,[62–70] thus they play a crucial role in determining plastic deformation of metal/ceramic multilayers, such as nucleation and gliding of lattice dislocations and their interactions with deposited dislocations at the interface. The NbC/Nb bicrystal model that adopts Baker-Nutting orientation relationship ($[100]_{NaCl}||[110]_{bcc}$ and $(001)_{NaCl}||(001)_{bcc}$)[32] was relaxed using molecular dynamics at 10 K (bcc = body centered crystal). Using atomically informed Frank-Bilby (AIFB) theory[71] we showed that the misfit dislocations are edge type with Burgers vectors $b_3 = \frac{\langle a \rangle}{4}[101]$ and $b_4 = \frac{\langle a \rangle}{4}[10\bar{1}]$ as well as the line senses along $[10\bar{1}]$ and $[101]$, respectively. A detailed study of the atomic stacking sequences of the unrelaxed interface reveals the existence of four types of regions T1 to T4 (Fig. 4a, b1–b4). In T1, niobium atoms in the Nb layer are at the top of the Nb atoms in the NbC layer. In the T3 region, Nb atoms in the Nb layer are at the top of C atoms in the NbC layer. The T2 and T4 regions show metastable regions where Nb atoms in the Nb layer are between the Nb and C atoms in the NbC layer. Because the Nb–C bonds are covalent and much stronger than the metallic bonds, they are energetically favored on the interface. Therefore, to a first-order approximation, the atomic stacks in T1 regions forming mostly Nb–Nb metallic bonds are not stable. Stacks in both T3 and T4 regions are stable as at these regions each Nb atoms in Nb layer forms one or two Nb–C bonds. After the interface relaxation (Fig. 4c), the unstable T1 regions are completely removed, whereas both T3 and T4 regions remain intact. These observations are in good agreement with the experimental, first-principles and modified embedded-atom method (MEAM) calculations of Fe/TiC (or TiN) interface where the region with Fe atoms on the top of C(N) atoms are energetically stable.[72] Figure 4c shows the plot of the disregistry vector[73] at the NbC–Nb interface after relaxation. Misfit dislocations can be
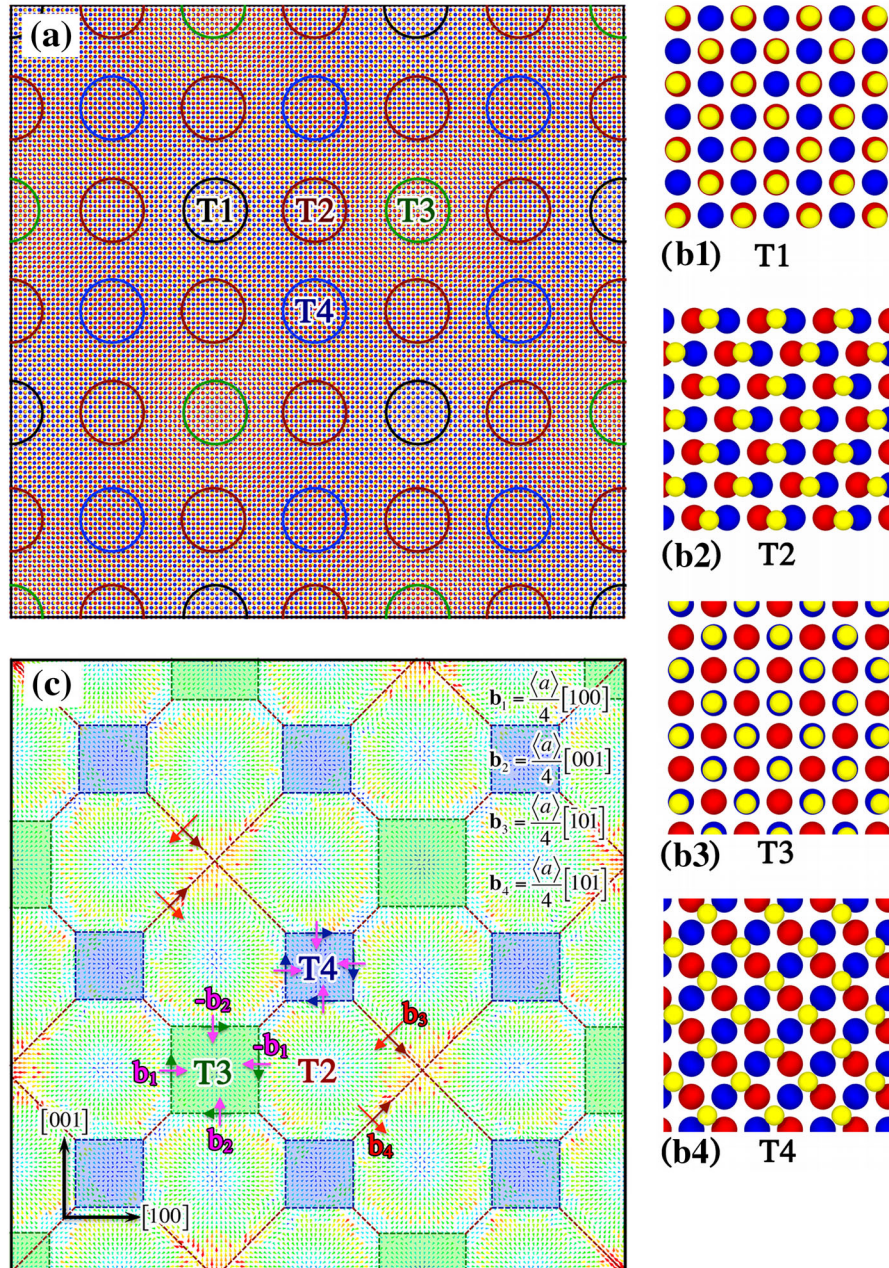
Fig. 4. (a) The *unrelaxed* NbC–Nb interface with four regions (T1–T4) identified according to the interface atomic stacking (see b1–b4). The lightest (yellow) circles denote the Nb atoms in Nb layer. The darker (red and blue) circles denote the Nb and C atoms in NbC layer, respectively. (b1–b4) different atomic stackings in NbC–Nb interface associated with regions T1–T4, respectively. (c) The plot of the disregistry analysis of the *relaxed* NbC–Nb interface. The dislocation lines and their Burgers vectors have been identified and marked. The plot is colored according to the disregistry magnitude.

seen in the interface where the disregistry vector changes abruptly to its mirror direction.[71] In agreement with the findings from AIFB, two sets of dislocation lines (b3 and b4) form along $\langle 110 \rangle$ directions. In addition, the T3 and T4 regions are enclosed by segmental misfit dislocations with Burgers vectors $\mathbf{b}_1$, $\mathbf{b}_2$, $-\mathbf{b}_1$, and $-\mathbf{b}_2$ (see Fig. 4c) and the line directions along $\langle 100 \rangle$. It is also interesting to note that the relaxed interface contains large areas of T2 regions despite the metastable

nature of the T2 stacks. This outcome may be attributed to the lower interface stacking fault energy of the T2 region than the core energy of an equivalent dislocation if this region is nonexistent.

Plastic Deformation Mechanisms

Figure 5a shows the compressive stress–strain curve for 3 nm NbC/7 nm Nb multilayer models being compressed normal to the interface. Defor-
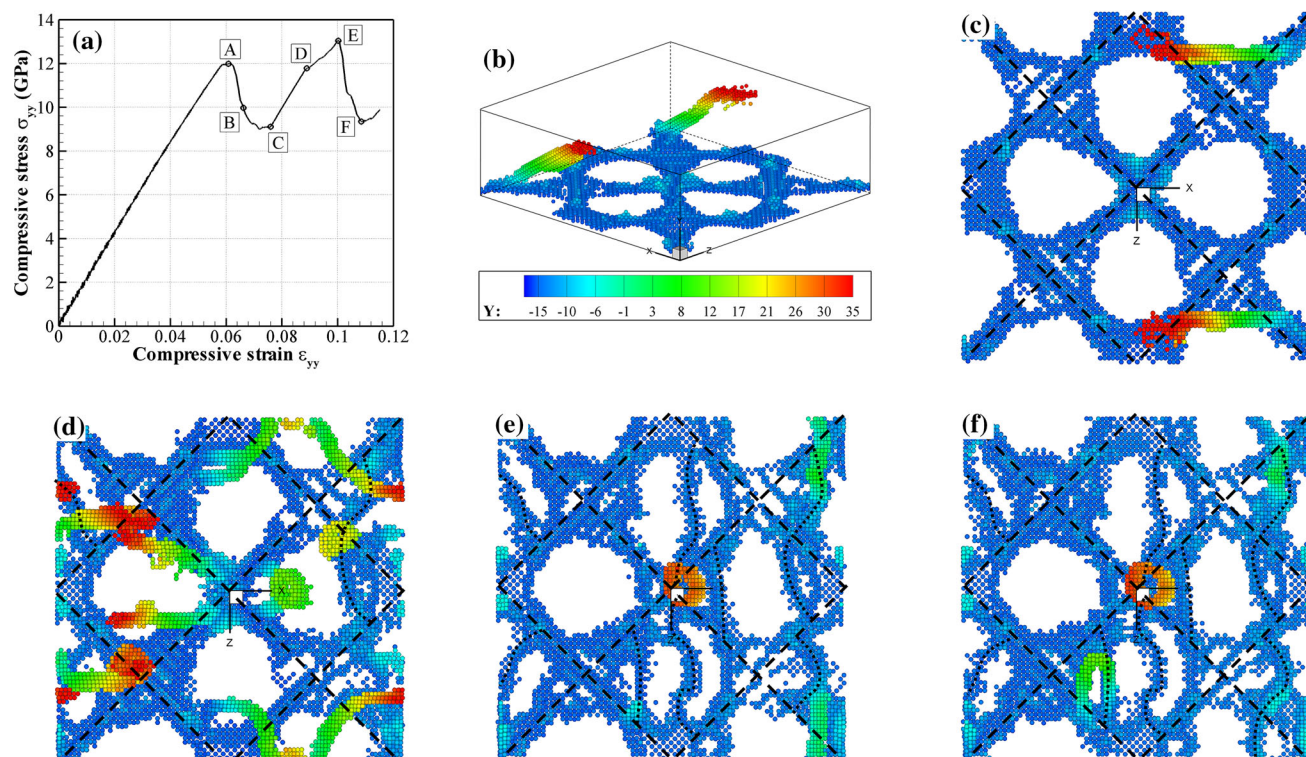
Fig. 5. (a) Stress–strain curve of 3 nm NbC/7 nm Nb under compressive loading normal to the interface. (b–f) Atomic structures with respect to the marked points in the stress–strain curve. Atoms in the Nb layer are colored according to the y coordinate. (b) and (c) At point A: Three-dimensional and top views of dislocations that nucleate from the misfit dislocations. (d) At point B: Dislocations propagation in the Nb layer (confined layer slip). (e) At point C: Dislocations annihilation in the Nb layer, deposited dislocations (dotted lines) at interface. (f) At point D: Nucleation of new dislocations from the misfit dislocations.[37]

mation is elastic up to a strain of 0.06 (point A) that coincides with the dislocation nucleation into the Nb layer from the interface (Fig. 5b, c). Dislocation propagation in the Nb layer results in a big burst in the stress–strain curve from point A to point C (Fig. 5d). Hardening from point C to E includes a linear section (CD) associating with annihilation of dislocations in the Nb layer (Fig. 5e) and a nonlinear section (DE) related to the incompatibility of plastic deformation in Nb and NbC, as well as the interaction between the propagating dislocations and the deposited and misfit dislocations (Fig. 5e, f). Finally, the stress drop from point E to F corresponds to slip transmission for dislocations from Nb to NbC and the formation of cracks in the NbC layer.

Effect of Layer Thickness Ratio

The effect of the metal/ceramic thickness ratio on the mechanical behavior of NbC/Nb multilayer composites has been explored for the constant bilayer period of 10 nm but different individual layer thicknesses: 5 nm NbC/5 nm Nb, 3 nm NbC/7 nm NbC, and 1 nm NbC/9 nm Nb. Wang and Misra[38] showed that increasing the metal/ceramic ratio and decreasing the distance between the deposited dislocations in the interface result in higher local shear stresses in the ceramic layer and lower compressive stresses in the metallic layer. Lower compressive stresses in the thicker metallic layer results in lower strain hardening and increase in the local stress in the ceramic layer facilitates the dislocation transmission into that layer. Figure 6 shows the stress–strain curves of the three samples, showing a lower strain-hardening rate for larger metal/ceramic thickness ratio which is in agreement with several studies including those by Wang and Misra[38] and Bhattacharyya et al.[3–5]

DISCUSSION

Studies have clarified the mechanisms of interactions of dislocations with the interface dislocations including the extrinsic (deposited) and intrinsic misfit dislocations. However, for thin layers, when the stress required to propagate a threading dislocation is higher than the nucleation stress, the nucleation of lattice dislocations from the interface becomes the main deformation mechanism. Therefore, a detailed study should be carried out on interface structure and its effect on the mechanisms of dislocation nucleation. Because of the mismatch between the thermal expansion coefficients of metal and ceramic layers, high residual stresses can be generated in both layers during the
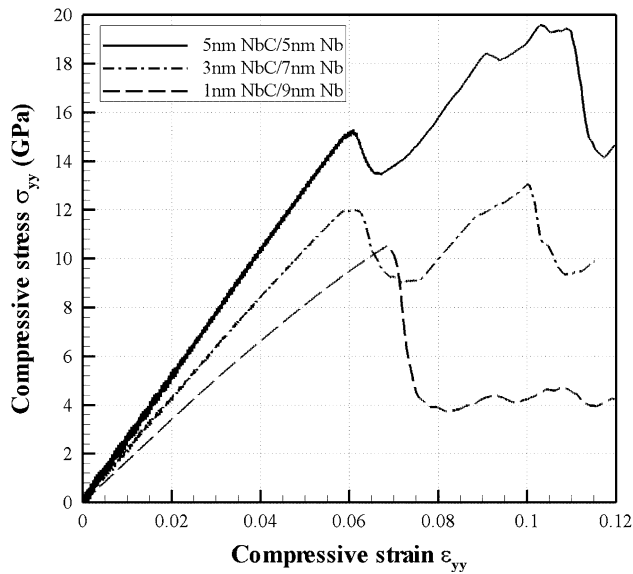
Fig. 6. Compressive stress–strain curves of NbC/Nb samples with 10 nm bilayer thickness and different individual layer thicknesses.[37]

deposition process.[74,75] Residual stresses may affect the pattern of the misfit dislocations and consequently impact the mechanical response of the multilayer composites. Molecular dynamics simulations are well suited for this type of problem.[76,77] On the other hand, structural and chemical defects may affect the interface properties including the interface structure and the interface strength. Changes in misfit dislocation patterns and dislocation nodes can impact the mechanical behavior of the multilayer composites as it is being controlled by the interfaces. Changes in interface strength may lead to improvement in toughness as the weak interface may deflect the cracks initiated in the ceramic layer.[20] Because of reliability issues of the available MEAM potentials, a detailed study of the effect of defects on the interface strength should be carried out using ab initio methods. A drawback of ab initio methods is their high computational cost that forces the model to include only coherent interfaces. Depending on the loading conditions, different nucleation mechanisms might be activated including the nucleation from misfit intersections in the T1 regions or dislocation segments surrounding the T3 regions. Providing the same stress field in the entire interface, uniform compression loading would determine which region is the preferred nucleation site. Positioning the highest shear stress at each region at the interface, nanoindentation is a practical tool to find the dislocation nucleation mechanisms for each region. Using uniaxial or biaxial loading, one can develop the yield locus for these nanocomposites and apply it to bridge the atomistic models to continuum models,[69,78] constructing a multiscale modeling framework.

CONCLUSION

In this article, we reviewed the literature with a focus on plastic deformation and strain hardening in metal/ceramic nanolayered composites. The main results related to experimental, theoretical, and atomistic modeling studies were summarized. We highlighted atomistic simulations of NbC/Nb nanolayered composites with a focus on interface structure, plastic deformation mechanisms, and effect of metal/ceramic thickness ratio on the mechanical response. Based on this work, several future directions have been suggested regarding the mechanical behavior of metal/ceramic layered composites with respect to experimental, theoretical, and modeling efforts.

REFERENCES

1. S.B. Sinnott and E.C. Dickey, *Mater. Sci. Eng. R Rep.* 43, 1 (2003).
2. G. Abadias, S. Dub, and R. Shmegera, *Surf. Coat. Technol.* 200, 6538 (2006).
3. D. Bhattacharyya, N.A. Mara, P. Dickerson, R.G. Hoagland, and A. Misra, *Philos. Mag.* 90, 1711 (2010).
4. D. Bhattacharyya, N.A. Mara, R.G. Hoagland, and A. Misra, *Scripta Mater.* 58, 981 (2008).
5. D. Bhattacharyya, N.A. Mara, P. Dickerson, R.G. Hoagland, and A. Misra, *Acta Mater.* 59, 3804 (2011).
6. M.B. Daia, P. Aubert, S. Labdi, C. Sant, F.A. Sadi, P. Houdy, and J.L. Bozet, *J. Appl. Phys.* 87, 7753 (2000).
7. K.K. Shih and D.B. Dove, *Appl. Phys. Lett.* 61, 654 (1992).
8. J.M. Lackner, W. Waldhauser, B. Major, L. Major, and M. Kot, *Thin Solid Films* 534, 417 (2013).
9. A. Dück, N. Gamer, W. Gesatzke, M. Griepentrog, W. Österle, M. Sahre, and I. Urban, *Surf. Coat. Technol.* 142–144, 579 (2001).
10. K.J. Ma, A. Bloyce, and T. Bell, *Surf. Coat. Technol.* 76–77, 297 (1995).
11. A. Madan, Y. Wang, S.A. Barnett, C. Engström, H. Ljungcrantz, L. Hultman, and M. Grimsditch, *J. Appl. Phys.* 84, 776 (1998).
12. A. Madan, X. Chu, and S.A. Barnett, *Appl. Phys. Lett.* 68, 2198 (1996).
13. S.A. Barnett and A. Madan, *Scripta Mater.* 50, 739 (2004).
14. A. Madan, S.A. Barnett, A. Misra, H. Kung, and M. Nastasi, *J. Vac. Sci. Technol., A* 19, 952 (2001).
15. S.A. Barnett, A. Madan, I. Kim, and K. Martin, *MRS Bull.* 28, 169 (2003).
16. G. Abadias, F. Pailloux, and S.N. Dub, *Surf. Coat. Technol.* 202, 3683 (2008).
17. G. Abadias, C. Tromas, Y.Y. Tse, and A. Michel, *Mater. Res. Soc. Symp. Proc.* 880 E, BB2.8 (2005).
18. C.H. Liu, W.-Z. Li, and H.-D. Li, *Nucl. Instrum. Methods Phys. Res. Sect.* B 95, 323 (1995).
19. J.L. He, W.Z. Li, H.D. Li, and C.H. Liu, *Surf. Coat. Technol.* 103–104, 276 (1998).

20. T.D. Moustakas, J. Scanlon, J.Y. Koo, H.W. Deckman, A. Ozekcin, R. Friedman, and J.A. McHenry, *Mater. Sci. Eng., B* 6, 179 (1990).
21. J. Wang, W.-Z. Li, H.-D. Li, B. Shi, and J.-B. Luo, *Thin Solid Films* 366, 117 (2000).
22. Z. Chen and J.J. Mecholsky, *J. Mater. Res.* 8, 2362 (1993).
23. A.T. Alpas, J.D. Embury, D.A. Hardwick, and R.W. Springer, *J. Mater. Sci.* 25, 1603 (1990).
24. I.W. Kim, A. Madan, M.W. Guruz, V.P. Dravid, and S.A. Barnett, *J. Vac. Sci. Technol., A* 19, 2069 (2001).
25. X. Wang, A. Kolitsch, F. Prokert, and W. Möller, *Surf. Coat. Technol.* 103–104, 334 (1998).
26. G.A. Zhang, Z.G. Wu, M.X. Wang, X.Y. Fan, J. Wang, and P.X. Yan, *Appl. Surf. Sci.* 253, 8835 (2007).
27. X. Deng, N. Chawla, K.K. Chawla, M. Koopman, and J.P. Chu, *Adv. Eng. Mater.* 7, 1099 (2005).
28. X. Deng, C. Cleveland, N. Chawla, T. Karcher, M. Koopman, and K.K. Chawla, *J. Mater. Eng. Perform.* 14, 417 (2005).
29. G. Tang, D.R.P. Singh, Y.-L. Shen, and N. Chawla, *Mater. Sci. Eng., A* 502, 79 (2009).
30. S. Lotfian, M. Rodríguez, K.E. Yazzie, N. Chawla, J. Llorca, and J.M. Molina-Aldareguía, *Acta Mater.* 61, 4439 (2013).
31. D.R.P. Singh, N. Chawla, G. Tang, and Y.-L. Shen, *Acta Mater.* 58, 6628 (2010).
32. P.L. Sun, J.P. Chu, T.Y. Lin, Y.L. Shen, and N. Chawla, *Mater. Sci. Eng., A* 527, 2985 (2010).
33. G. Tang, Y.-L. Shen, D.R.P. Singh, and N. Chawla, *Acta Mater.* 58, 2033 (2010).
34. S. Lotfian, J.M. Molina-Aldareguia, K.E. Yazzie, J. Llorca, and N. Chawla, *Philos. Mag. Lett.* 92, 362 (2012).
35. Y.-L. Shen, C.B. Blada, J.J. Williams, and N. Chawla, *Mater. Sci. Eng., A* 557, 119 (2012).
36. A.A. Voevodin and J.S. Zabinski, *Diam. Relat. Mater.* 7, 463 (1998).
37. P.M. Anderson and C. Li, *Nanostructured Mater.* 5, 349 (1995).
38. J. Wang and A. Misra, *Curr. Opin. Solid State Mater. Sci.* 18, 19 (2014).
39. W.D. Nix, *Math. Mech. Solids* 14, 207 (2009).
40. P.M. Anderson and E.R. Kreidler, *Mater. Res. Soc. Symp. Proc.* 505, 571 (1997).
41. E.R. Kreidler and P.M. Anderson, *Mater. Res. Soc. Symp. Proc.* 434, 159 (1996).
42. J.D. Embury and J.P. Hirth, *Acta Metall. Mater.* 42, 2051 (1994).
43. S.I. Rao and P.M. Hazzledine, *Philos. Mag. A* 80, 2011 (2000).
44. J. Wang, R.G. Hoagland, J.P. Hirth, and A. Misra, *Acta Mater.* 56, 5685 (2008).
45. A. Levay, G. Möbus, V. Vitek, M. Rühle, and G. Tichy, *Acta Mater.* 47, 4143 (1999).
46. D.J. Siegel, L.G. Hector Jr., and J.B. Adams, *Acta Mater.* 50, 619 (2002).
47. D.J. Siegel, L.G. Hector, and J.B. Adams, *Phys. Rev. B* 65, 085415 (2002).
48. D.J. Siegel (Ph.D. Dissertation, University of Illinois at Urbana-Champaign, 2001).
49. A. Arya and E.A. Carter, *J. Chem. Phys.* 118, 8982 (2003).
50. L.M. Liu, S.Q. Wang, and H.Q. Ye, *J. Phys.: Condens. Matter* 16, 5781 (2004).
51. W.-S. Jung and S.-H. Chung, *Model. Simul. Mater. Sci. Eng.* 18, 075008 (2010).
52. H. Sawada, S. Taniguchi, K. Kawakami, and T. Ozaki, *Model. Simul. Mater. Sci. Eng.* 21, 045012 (2013).
53. R. Benedek, D.N. Seidman, M. Minkoff, L.H. Yang, and A. Alavi, *Phys. Rev. B* 60, 16094 (1999).
54. R. Benedek, A. Alavi, D.N. Seidman, L.H. Yang, D.A. Muller, and C. Woodward, *Phys. Rev. Lett.* 84, 3362 (2000).
55. S. Tanaka, R. Yang, and M. Kohyama, *Philos. Mag.* 86, 5123 (2006).
56. A. Christensen and E.A. Carter, *J. Chem. Phys.* 114, 5816 (2001).
57. Y. Long and N.X. Chen, *Comput. Mater. Sci.* 42, 426 (2008).
58. S.K. Yadav, R. Ramprasad, A. Misra, and X.-Y. Liu, *J. Appl. Phys.* 111, 083505 (2012).
59. N.-Y. Park, J.-H. Choi, P.-R. Cha, W.-S. Jung, S.-H. Chung, and S.-C. Lee, *J. Phys. Chem. C* 117, 187 (2013).
60. X. Luo, G. Qian, E.G. Wang, and C. Chen, *Phys. Rev. B* 59, 10125 (1999).
61. S.V. Dmitriev, N. Yoshikawa, M. Kohyama, S. Tanaka, R. Yang, and Y. Kagawa, *Acta Mater.* 52, 1959 (2004).
62. A.P. Sutton and R.W. Balluffi, *Interfaces in Crystalline Materials* (Oxford, U.K.: Oxford University Press, 2007).
63. D.E. Spearot, K.I. Jacob, and D.L. McDowell, *Int. J. Plast.* 23, 143 (2007).
64. P.M. Derlet, P. Gumbsch, R. Hoagland, J. Li, D.l. McDowell, H. Van Swygenhoven, and J. Wang, *MRS Bull.* 34, 184 (2009).
65. I.N. Mastorakos, H.M. Zbib, and D.F. Bahr, *Appl. Phys. Lett.* 94, 173114 (2009).
66. H.M. Zbib, C.T. Overman, F. Akasheh, and D.F. Bahr, *Int. J. Plast.* 27, 1618 (2011).
67. I.J. Beyerlein, N.A. Mara, J. Wang, J.S. Carpenter, S.J. Zheng, W.Z. Han, R.F. Zhang, K. Kang, T. Nizolek, and T.M. Pollock, *JOM* 64, 1192 (2012).
68. S. Shao, H.M. Zbib, I.N. Mastorakos, and D.F. Bahr, *J. Appl. Phys.* 112, 044307 (2012).
69. N. Abdolrahim, H.M. Zbib, and D.F. Bahr, *Int. J. Plast.* 52, 33 (2014).
70. J. Wang, R.F. Zhang, C.Z. Zhou, I.J. Beyerlein, and A. Misra, *Int. J. Plast.* 53, 40 (2014).
71. J. Wang, R. Zhang, C. Zhou, I.J. Beyerlein, and A. Misra, *J. Mater. Res.* 28, 1646 (2013).
72. H.-K. Kim, W.-S. Jung, and B.-J. Lee, *Acta Mater.* 57, 3140 (2009).
73. R.G. Hoagland, J.P. Hirth, and A. Misra, *Philos. Mag.* 86, 3537 (2006).
74. V. Teixeira, *Thin Solid Films* 392, 276 (2001).
75. J.H. Lee, W.M. Kim, T.S. Lee, M.K. Chung, B. Cheong, and S.G. Kim, *Surf. Coat. Technol.* 133–134, 220 (2000).
76. I. Salehinia, J. Wang, D.F. Bahr, and H.M. Zbib, *Int. J. Plast.* 59, 119 (2014).
77. S. Shao, H.M. Zbib, I. Mastorakos, and D.F. Bahr, *J. Eng. Mater. Technol.* 135, 021001 (2013).
78. J. Wang, C. Zhou, I.J. Beyerlein, and S. Shao, *JOM* 66, 102 (2014).